

# NH<sub>3</sub>-promoted hydrolysis of NO<sub>2</sub> induces explosive growth in HONO

Wanyun Xu<sup>1</sup>, Ye Kuang<sup>2,\*</sup>, Chunsheng Zhao<sup>3</sup>, Jiangchuan Tao<sup>2</sup>, Gang Zhao<sup>3</sup>, Yuxuan Bian<sup>4</sup>,  
Wen Yang<sup>5</sup>, Yingli Yu<sup>3</sup>, Chuanyang Shen<sup>3</sup>, Linlin Liang<sup>1</sup>, Gen Zhang<sup>1</sup>, Weili Lin<sup>6</sup>,  
Xiaobin Xu<sup>1</sup>

<sup>1</sup> State Key Laboratory of Severe Weather, Key Laboratory for Atmospheric Chemistry, Institute of Atmospheric Composition, Chinese Academy of Meteorological Sciences, Beijing, 100081, China.

<sup>2</sup> Institute for Environmental and Climate Research, Jinan University, Guangzhou, China.

<sup>3</sup> Department of Atmospheric and Oceanic Sciences, School of Physics, Peking University, Beijing, China

<sup>4</sup> State Key Laboratory of Severe Weather, Chinese Academy of Meteorological Sciences, Beijing, 100081, China

<sup>5</sup> State Key Laboratory of Environmental Criteria and Risk Assessment, Chinese Research Academy of Environmental Sciences, Beijing, 100081, China

<sup>6</sup> College of Life and Environmental Sciences, Minzu University of China, Beijing, 100081, China

Corresponding author: Ye Kuang (kuangye@jnu.edu.cn)

## Abstract

The study of atmospheric nitrous acid (HONO), which is the primary source of OH radicals, is crucial to atmospheric photochemistry and heterogeneous chemical processes. The heterogeneous NO<sub>2</sub> chemistry under haze conditions was pointed out to be one of the missing sources of HONO on the North China Plain, producing sulfate and nitrate in the process. However, controversy exists between various proposed mechanisms, mainly debating on whether SO<sub>2</sub> directly takes part in the HONO production process and what roles NH<sub>3</sub> and the pH value play in it. In this paper, never before seen explosive HONO production (maximum rate: 16 ppb h<sup>-1</sup>) was reported and evidence was found for the first time in field measurements during fog episodes (usually with 4<pH<6) and haze episodes under high relative humidity (pH≈4), that NH<sub>3</sub> was the key factor that promoted the hydrolysis of NO<sub>2</sub>, leading to explosive growth of HONO and nitrate under both high and lower pH conditions. The results also suggest that SO<sub>2</sub> takes minor or insignificant part in the HONO formation during fog and haze events, but was indirectly oxidized upon the photolysis of HONO through subsequent radical mechanisms. Aerosol hygroscopicity significantly increased with the rapid inorganic secondary aerosol formation further promoting the HONO production as a positive feedback. For future photochemical and aerosol pollution abatement, it is crucial to introduce

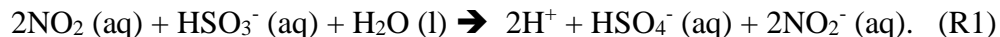
effective NH<sub>3</sub> emission control measures, since the NH<sub>3</sub>-promoted NO<sub>2</sub> hydrolysis is a large daytime HONO source, releasing large amounts of OH radicals upon photolysis, which will contribute largely to both atmospheric photochemistry and secondary aerosol formation.

## 1 Introduction

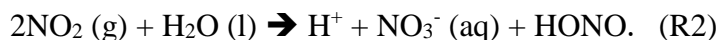
Nitrous acid (HONO) plays a vital role in atmospheric chemistry due to the fact that its photolysis is a major source (Michoud et al., 2014; Kleffmann et al., 2005) of hydroxyl radical (OH) which determines the atmospheric oxidative capacity and plays crucial role in tropospheric chemistry in processes such as the ozone formation, the degradation of volatile organic compounds and the secondary aerosol formation (Cheng et al., 2016; Wang et al., 2016). Hence, the source study of nitrous acid (HONO) is of crucial importance for the understanding of the tropospheric chemistry, for chemistry and climate modelling and for developing effective pollution control strategies (Lu et al., 2018).

The North China Plain (NCP) is troubled by the persistent complex air pollution with high loadings of both photochemical pollutants and particulate pollution (Zheng et al., 2015; Ran et al., 2011) and the simultaneous mitigation of the two types of pollution has encountered trouble due to the nonlinear dependence of ozone on NO<sub>x</sub> (Xing et al., 2018). Unknown daytime sources of HONO caught attention during the past few years (Michoud et al., 2014; Liu et al., 2014; Su et al., 2011) and results from a recent study indicate that an additional missing source is required to explain more than 50% of observed HONO concentration in the daytime in Western China (Huang et al., 2017). Results from several recent studies demonstrate that intense heterogeneous conversion of NO<sub>2</sub> to HONO on particle surfaces might be a significant source of HONO (Liu et al., 2014; Cui et al., 2018).

Two main HONO heterogeneous production pathways involving aerosol water and NO<sub>2</sub> were proposed. In light of drastic decrease of solar radiation during severe haze events and rich ammonia conditions on the NCP, the first pathway hypothesized that NO<sub>2</sub> (g) dissolved in aerosol water at aerosol pH > 5.5 rapidly formed HONO while oxidizing HSO<sub>3</sub><sup>-</sup> (aq) to sulfate. The stoichiometry of this mechanism is as follows (Cheng et al., 2016; Wang et al., 2016):



Based on this mechanism, good agreement between modelled and observed sulfate formation rates were achieved. However, the assumption that the pH of ambient aerosols can reach beyond 5.5 is a debatable issue. Results from several most recent studies indicate that the pH of ambient aerosols fall in the range of 3-5 in most cases (Ding et al., 2018;Liu et al., 2017a;Song et al., 2018). Given this, it was proposed that HONO and NO<sub>2</sub><sup>-</sup> were produced in the hydrolysis process of NO<sub>2</sub>, releasing OH radicals upon photolysis, which indirectly oxidize SO<sub>2</sub> to sulfate (Li et al., 2018b):



Results of Yabushita et al. (2009) suggest that anions (such as Cl<sup>-</sup>, Br<sup>-</sup> and I<sup>-</sup>) greatly enhance the hydrolysis of NO<sub>2</sub> on water, and the NO<sub>2</sub> uptake coefficients of R2 can be enhanced several orders of magnitude by increasing electrolyte concentration. The ambient aerosol particles in the boundary layer are in aqueous phase under high RH (Liu et al., 2017b) and the aerosol or fog water is not pure with different dissolved anions (Wu et al., 2018;Lu et al., 2010). Therefore, HONO and nitrate formed through this mechanism should be independent of aerosol acidity, and should be primarily affected by the aerosol surface area density, aerosol liquid water content and NO<sub>2</sub> concentration (Li et al., 2018b). Moreover, recent theoretical simulations have proposed a HONO formation mechanism involving NO<sub>2</sub> and water and have identified that NH<sub>3</sub> can promote the hydrolysis of NO<sub>2</sub> (Li et al., 2018a) (R2). Despite of this, no direct evidence from field observations were available in this paper to support their findings.

Although the proposed HONO formation mechanisms are all heterogeneous reactions of NO<sub>2</sub>, the details of how SO<sub>2</sub>, pH and NH<sub>3</sub> are involved in heterogeneous formation are still under debate (Li et al., 2018b) and a clear mechanism is still missing in current models to explain both the daytime concentration of observed HONO and the secondary inorganic aerosol formation. Measurements of HONO are rare and simultaneous observations of HONO and aerosol physical and chemical characteristics are lacking to thoroughly analyze or directly support the aerosol heterogeneous HONO formation mechanisms involving NO<sub>2</sub>. In this paper, we present for the first time simultaneous measurements of HONO, sulfate and nitrate as well as other precursor gases, oxidants and meteorological parameters during both fog and haze episodes under high ambient RH. Fog water pH is usually greater than 5.5 in eastern China (Safai et al., 2008;Lu et al., 2010), while calculations in this work and previous studies collectively indicate a moderately acidic

condition ( $4 < \text{pH} < 5$ ) for fine particles in northern China winter haze. The observational results unveil that  $\text{NH}_3$  is the key factor that promotes the hydrolysis of  $\text{NO}_2$ , resulting in explosive formation of HONO, nitrate and sulfate.

## 2 Site description and instruments

From 15<sup>th</sup> Oct. to 25<sup>th</sup> Nov. 2016, a field campaign intended to study sulfate formation was conducted at the Ecological and Agricultural Meteorology Station ( $39^\circ 09' \text{N}$ ,  $115^\circ 44' \text{E}$ ) of the Chinese Academy of Meteorological Sciences. The site is partly composed of experimental farmland and is also surrounded by farmland and small residential towns (nearest town  $\sim 1.5$  km). It is located between Beijing ( $\sim 100$  km) and Baoding ( $\sim 40$  km), two megacities on the North China Plain (Fig. 1). During this field campaign, an In situ Gas and Aerosol Compositions Monitor (IGAC, Fortelice International Co., Taiwan) was used for monitoring water-soluble ions ( $\text{Na}^+$ ,  $\text{K}^+$ ,  $\text{Ca}^{2+}$ ,  $\text{Mg}^{2+}$ ,  $\text{NH}_4^+$ ,  $\text{SO}_4^{2-}$ ,  $\text{NO}_3^-$ ,  $\text{NO}_2^-$ ,  $\text{Cl}^-$ ) of  $\text{PM}_{2.5}$  (particulate matter with aerodynamic diameter less than  $2.5 \mu\text{m}$ ) and trace gases including HONO,  $\text{SO}_2$ ,  $\text{NH}_3$ ,  $\text{HCl}$ , and  $\text{HNO}_3$  with a time resolution of 1 h. The IGAC system draws in ambient air through a  $\text{PM}_{10}$  inlet and passes the sample through a sharp-cut  $\text{PM}_{2.5}$  cyclone at a flowrate of  $16.7 \text{ L min}^{-1}$ . The total length of the stainless steel sampling line is approximately 2 m, with an inner diameter of 3.18 cm (1.25 inch), resulting in a residence time below 6 s, suggesting that underestimates in  $\text{NH}_3$  possibly caused by adsorption on the stainless steel sampling tube as was proposed by Young et al. (2016) might be unimportant. A vertical annular denuder wetted with dilute  $\text{H}_2\text{O}_2$  solution ( $5 \times 10^{-3} \text{ M}$ ) collects the trace gases and converts  $\text{SO}_2$  rapidly to  $\text{SO}_4^{2-}$ , preventing  $\text{SO}_2$  from reacting with  $\text{NO}_2$  in the absorption solution to produce HONO artefacts. A scrub and impact aerosol collector under the denuder is mounted at an inclined angle to capture particles based on impaction after condensation growth. Two separate Ion Chromatographs are used to respectively analyze anions and cations for the gas and aerosol liquid extracts which were injected from the denuder and the aerosol collector once an hour. The detection limits are below  $0.12 \mu\text{g m}^{-3}$  and the background concentration of most water-soluble inorganic ions within the instrument were below  $0.11 \mu\text{g m}^{-3}$ , only with  $\text{SO}_4^{2-}$  showing a background concentration of  $1.10 \mu\text{g m}^{-3}$  (Young et al., 2016). Considering the severe pollution state the NCP is under, these measurement uncertainties are fully acceptable. The instrument has shown good performance in the past, agreeing well with filter based samples (Liu et al., 2017a). Standard LiBr solution was continuously added to the aerosol liquid extracts during

the measurements, to ensure the sampling and analyzing process is stable. The swing amplitude was within the range of three standard deviation, confirming the stability of the ion analyzing system throughout the campaign. A mixed standard solution was diluted to perform multipoint calibrations (at 5, 10, 20, 50, 100, 200, 500 and 1000 ppb concentrations) at the beginning and at the end of the campaign for the ions  $\text{Na}^+$ ,  $\text{K}^+$ ,  $\text{Ca}^{2+}$ ,  $\text{Mg}^{2+}$ ,  $\text{NH}_4^+$ ,  $\text{Li}^+$ ,  $\text{SO}_4^{2-}$ ,  $\text{NO}_3^-$ ,  $\text{NO}_2^-$ ,  $\text{Cl}^-$ ,  $\text{Br}^-$ , with the  $R^2$  of the calibrations reaching above 0.9999. A comparison between  $\text{NH}_3$  observed by IGAC and by an economical  $\text{NH}_3$  analyser (LGR, DLT-100, details see Meng et al. (2018)) yielded an overall slope of 0.91 with  $R=0.63$  (Fig.S1a). A better comparison result (slope of 1.03,  $R=0.74$ ) would be obtained if data associated with  $\text{RH} \geq 80$  were excluded (Fig.S1b). The overestimation of LGR instruments compared to denuder based instruments has also been reported in Teng et al. (2017), suggesting possible interference of water vapor on  $\text{NH}_3$  measurements. As can be seen in Fig.S2, both instruments captured the same the diurnal variation of  $\text{NH}_3$  during the four case episodes in this study, which proves that the IGAC instrument was able to capture the overall variation trends of  $\text{NH}_3$ . Since both instruments have their uncertainties, we decided to use the  $\text{NH}_3$  measured by the IGAC instrument for better consistency with the other data.

$\text{NO}_x$  and CO were observed using commercial instruments from Thermo Electronics (Model 42CTL and 48CTL), while the Aerolaser AL2021  $\text{H}_2\text{O}_2$ -monitor was used to measure  $\text{H}_2\text{O}_2$  concentrations. The ambient RH, temperature, wind speed and wind direction were observed using an automatic weather station. The dry state particle number size distributions (PNSDs) in the diameter range of 3nm to  $10\mu\text{m}$ , were jointly measured by a scanning mobility particle size spectrometer (SMPS) and an Aerodynamic Particle Sizer (APS, TSI Inc., Model 3321). The ambient aerosol liquid water concentrations were calculated based on measurements of a three-wavelength humidified nephelometer system (Kuang et al., 2018). The aerosol hygroscopicity parameter  $\kappa$  (Petters and Kreidenweis, 2007) is calculated using the method proposed by Kuang et al. (2017).

### **3 Observed simultaneous rapid increase of HONO, nitrate and sulfate**

The time series of HONO, sulfate, nitrate and ammonium and precursor gases, meteorological parameters and other parameters are shown in Fig. 2. During this observation period, HONO concentration ranged from 0.31 to 17.6 ppb (ranged from 0.3 to 6.0 ppb during most periods) with an average of 3.0 ppb. The HONO/ $\text{NO}_2$  ratio ranged from 0.03 to 0.75 with an

average of 0.18, which is higher than the average HONO/NO<sub>2</sub> ratio previously observed in China (Liu et al., 2014; Cui et al., 2018). NO<sub>2</sub> concentration ranged from 7.5 to 60.1 ppb with an average of 32.0 ppb. NH<sub>3</sub> concentration ranged from 0.05 to 30 ppb with an average of 12.3 ppb. Four rapid HONO formation events were identified in Fig.2, two under foggy conditions and the other two under high RH conditions.

### 3.1 Explosive growth of HONO during fog episodes

Two dense fog episodes with rapid HONO increase were observed for the first time in China, occurring on the 4<sup>th</sup> and 5<sup>th</sup> Nov. 2016. From satellite images (Fig. 1) it can be seen that on the 5<sup>th</sup> Nov., a wide area of the NCP was shrouded by fog before noon (about 11:30) including the observation site, however, the fog area reduced in the afternoon (about 13:30) and dissipated near the observation site. The evolution of the fog-shrouded area during these two days was also observed by a geostationary satellite (<http://www.eorc.jaxa.jp/ptree/index.html>). These two fog episodes offer us a great opportunity to study the hydrolysis process of NO<sub>2</sub> (R2) and the role of SO<sub>2</sub> in heterogeneous HONO production in fog water (R1), which usually show pH above 5.5 (Safai et al., 2008; Lu et al., 2010).

The time series of simultaneously observed meteorological parameters, concentrations of nitrate, ammonium, sulfate and their precursor gases SO<sub>2</sub>, NO<sub>2</sub>, NO and NH<sub>3</sub>, as well as atmospheric oxidants such as O<sub>3</sub>, H<sub>2</sub>O<sub>2</sub> and other parameters including CO, which is indicative of transport processes during the two days with fog episodes are shown in Fig. 3. From 0:00 (Beijing local time) on the 4<sup>th</sup> Nov., the ambient RH continuously increased and reached 100% near 5:00, and lasted about 8.5 hours before it dropped below 100% near 13:30. However, at 15:30, the ambient RH began to rise again and reached 100% near 19:30, and then sustained until 12:00 on the 5<sup>th</sup> Nov. The latter fog episode lasted about 18.5 hours.

During the first fog episode, the rapid increases of HONO, nitrate, sulfate and ammonium were observed from 8:50 to 11:30 (Case1). HONO increased from 3.6 ppb to 10.6 ppb, with the most rapid increase occurring around 11:00 at a rate of 5.5 ppb h<sup>-1</sup>. During the HONO increasing period, the variation characteristics of related trace gases and other parameters are as follows. NH<sub>3</sub> concentration increased slowly at first and then increased drastically near 11 am (10 ppb h<sup>-1</sup>). SO<sub>2</sub> concentration remained almost constant at first and then increased from near 0.25 ppb to 0.4 ppb. NO<sub>2</sub> concentration increased continuously with a small magnitude, while NO concentration

increased first and then decreased.  $\text{H}_2\text{O}_2$  concentration is continuously increasing, but  $\text{O}_3$  concentration remained near zero. CO concentration remained almost constant ( $\sim 2.5$  ppm), suggesting that there was no evident plume transport during this process. Wind speed was less than  $2 \text{ m s}^{-1}$ , and dropped almost to  $0 \text{ m s}^{-1}$  when HONO concentration dramatically increased, further supporting the fact that the drastic increase was not caused by transport processes. Ammonium, nitrate and sulfate concentration steadily increased from 7.5, 13.2,  $13.7 \mu\text{g m}^{-3}$  to 14.3, 30.4,  $31.0 \mu\text{g m}^{-3}$ , respectively. A noticeable increase in nitrite was also observed, when HONO increased most rapidly. It should be noted that the cutting diameter of the IGAC instrument is  $2.5 \mu\text{m}$ , which means that observed concentrations only represent the variation of inorganics ions in aerosol water, and that of fog droplets were not included.

During the second fog episode, HONO, nitrate, sulfate and ammonium started to increase rapidly from 9:30 and reached a plateau near 12:30, when the fog started to dissipate (Case2). HONO increased from 3 ppb to 9.5 ppb, with the fastest increase occurring near 11:00 at a rate of  $3.5 \text{ ppb h}^{-1}$ . Variation characteristics of other parameters are as follows.  $\text{NH}_3$  concentration increased steadily from 5 ppb to 24 ppb.  $\text{SO}_2$  concentration increased steadily from 0.25 ppb to 1.25 ppb.  $\text{NO}_2$  concentration remained almost constant at the very beginning (near 40 ppb) and then increase slightly, while NO concentration remained almost constant (near 30 ppb) throughout the entire fog period.  $\text{H}_2\text{O}_2$  concentration increased slightly at first and then rose rapidly towards the end of the fog period.  $\text{O}_3$  concentration increased very slightly. CO concentration remained also near constant ( $\sim 3$  ppm). Wind speed was steady and less than  $2 \text{ m s}^{-1}$  at the beginning, however, began to increase quickly at noon. Ammonium, nitrate and sulfate concentration steadily grew from 8.1, 17,  $3.8 \mu\text{g m}^{-3}$  to 15.3, 39.3,  $8.0 \mu\text{g m}^{-3}$ , respectively. The variation of nitrite was very similar to that of HONO. The variation of wind speed demonstrate that at the very beginning of the HONO increase, the air mass was relatively stagnant, but became windy when the fog dissipated.

### **3.2 Explosive growth of HONO during haze episodes with high RH conditions**

The two periods with rapid HONO increase under high RH conditions occurred on the 11<sup>th</sup> and 14<sup>th</sup> Nov., respectively. The time series of simultaneously observed meteorological parameters, concentrations of nitrate, ammonium, sulfate and their precursor gases  $\text{SO}_2$ ,  $\text{NO}_2$ , NO and  $\text{NH}_3$ , as well as oxidants including  $\text{O}_3$ ,  $\text{H}_2\text{O}_2$  and other parameters such as CO concentration, aerosol

volume concentration in dry state and aerosol liquid water content during the two days are shown in Fig.4.

On the 11<sup>th</sup> Nov., HONO started rising from 6:30 (3.4 ppb) and came to a halt at 9:00 (11.5 ppb) (Case 3). The quickest increase of HONO occurred near 9 o'clock with a rate of 5.6 ppb h<sup>-1</sup>. The key features of other parameters are introduced in the following. The ambient RH decreased rapidly (from foggy condition to near 75%). NH<sub>3</sub> increased slowly at first and then grew rapidly. NO<sub>2</sub> increased slowly and SO<sub>2</sub> remained low. The total volume concentration of PM<sub>2.5</sub> was decreasing. Ammonium, nitrate and sulfate concentrations increased very slowly at first and then evident increase was observed in ammonium and nitrate. The decrease in dry state volume concentration of PM<sub>2.5</sub> demonstrate that the air mass is not quite steady due to transport or boundary layer processes. The slight increase of nitrate and sulfate despite the drop in total PM<sub>2.5</sub> concentration suggest that the nitrate and sulfate produced during the increasing process of HONO outgrew those lost to boundary layer mixing and transport.

On the 14<sup>th</sup> Nov., HONO increased drastically near 11:00, reaching 17.6 ppb at 11:30 (16.1 ppb h<sup>-1</sup>) and then dropped promptly to 4 ppb at 12:30 (Case 4). This phenomenon took place when the fog dissipated and the ambient RH abruptly dropped to near 85%. Key variation features of other parameters are as follows. NH<sub>3</sub> increased rapidly from 9.7 ppb to 30 ppb. NO<sub>2</sub> concentration was increasing quickly, while SO<sub>2</sub> concentration remained low. The concentration of sulfate and nitrate also increased quickly. Volume concentration of PM<sub>2.5</sub> was decreasing, indicating that even more sulfate and nitrate were formed than the observed growth in their concentrations. The photolysis of HONO was high probably the cause for its drastic decrease. Note that the HONO was not increasing during the period where only NO<sub>2</sub> increased rapidly and NH<sub>3</sub> varied little.

## 4 Discussions

### 4.1 HONO budget analysis

In these four rapid HONO increasing episodes, the maximum HONO growth rates (d[HONO]/dt) all exceed 5 ppb h<sup>-1</sup>, and even reach beyond 16 ppb h<sup>-1</sup>. Such high HONO growth rates as observed in this study were not yet reported in literature. In this section, we discuss whether these HONO formation events can be explained by current known mechanisms and which mechanisms are determining the variation of HONO.



The net HONO production rate can be estimated by accounting for all the currently known sources and sinks using the following equation:

$$P_{HONO}^{net} = P_{emi} + P_{hom}^{net} + P_{het} - L_{pho} - L_{dep}, \quad (\text{Eq.1})$$

where  $P_{emi}$  is the total emission rate of HONO,  $P_{hom}^{net}$  the net HONO production in homogenous gas phase reactions,  $P_{het}$  the HONO produced via heterogeneous reactions,  $L_{pho}$  the loss of HONO due to photolysis and  $L_{dep}$  the loss of HONO due to deposition.

Previous studies have shown that HONO can be emitted through biomass burning and vehicles (Nie et al., 2015; Huang et al., 2017). Biomass burning contributes to HONO mainly by increasing particle surface area and NO<sub>2</sub> conversion efficiency (Nie et al., 2015). Under foggy conditions, surface area was not the limiting factor to the NO<sub>2</sub> conversion. During the haze events, particle surface area was decreasing due to decreasing humidity and aerosol water content. Hence, the variation of surface area cannot explain the observed HONO increases. According to the mapped fire spots on the days of the HONO events (Fig.S3), there was no fire within 20 km distance to the site. K<sup>+</sup> is often used as an indicator for biomass burning. The average K<sup>+</sup> concentration during the whole campaign ranged from 0.022 to 5.95 µg m<sup>-3</sup>, with an average of 1.28 µg m<sup>-3</sup>. The K<sup>+</sup> level during the four events were 1.39, 1.08, 1.51 and 1.54 µg m<sup>-3</sup>, respectively, showing no evident sign of biomass burning. Hence, only vehicle emissions were considered in this study.

Vehicle emissions can be estimated using the following equation:

$$P_{vehicle} = R_{emission} \times [NO_x]_{vehicle}, \quad (\text{Eq.2})$$

where  $R_{emission}$  is the vehicle emission ratio and  $[NO_x]_{vehicle}$  the NO<sub>x</sub> concentration from vehicle emissions. The NO/NO<sub>x</sub> ratio during the HONO increasing episodes ranged from 0.37 to 0.76, suggesting that the air masses were relatively aged compared to freshly emitted air mass from exhaust (NO/NO<sub>x</sub>>0.9). Here,  $P_{vehicle}$  is estimated assuming all the measured NO<sub>x</sub> came from vehicle emissions and an emission ratio of 1%, which is higher than the upper limit of 0.8% used in Huang et al. (2017), to obtain an upper limit for vehicle emissions.

HONO can be formed in gas phase reactions of NO with OH radicals and is lost through direct reactions with OH radicals. The net production of HONO via homogeneous reactions can be estimated using the equation:

$$P_{hom}^{net} = k_{NO+OH}[NO][OH] - k_{HONO+OH}[HONO][OH], \quad (\text{Eq. 3})$$

where  $k_{NO+OH}$  ( $7.2 \times 10^{-12} \text{ cm}^{-3} \text{ s}^{-1}$ ) and  $k_{HONO+OH}$  ( $5.0 \times 10^{-12} \text{ cm}^{-3} \text{ s}^{-1}$ ) are the rate constants of the reactions of NO and HONO with OH, at 298 K, respectively (Li et al., 2012). The diurnal variation of OH concentrations was inferred from Whalley et al. (2015), replacing OH under fog conditions with  $1 \times 10^5 \text{ cm}^{-3}$ .

Heterogeneous conversion of  $\text{NO}_2$  on aerosol and ground surface is considered a major source for HONO. However, the detailed mechanism (R1 or R2?) is still under debate and different studies have shown a large variability in the range of estimated  $\text{NO}_2$  uptake coefficient. Typically, the conversion of  $\text{NO}_2$  on aerosol and ground surface is parameterized as a linear function of  $\text{NO}_2$  uptake coefficients and surface to volume ratios (surface area densities) (Xue et al., 2014; Li et al., 2018b):

$$P_{het} = (k_g + k_a)[\text{NO}_2], \quad (\text{Eq.4-1})$$

$$k_g = \frac{1}{8} \cdot \vartheta_{\text{NO}_2} \cdot \gamma_g \cdot \frac{S}{V}, \quad (\text{Eq.4-2})$$

$$k_a = \frac{1}{4} \cdot \vartheta_{\text{NO}_2} \cdot \gamma_a \cdot S_a, \quad (\text{Eq.4-3})$$

where  $\vartheta_{\text{NO}_2}$  stands for the mean molecular speed,  $\gamma_g$  and  $\gamma_a$  for the uptake coefficient on ground and aerosol surface,  $S/V$  for the surface to volume ratio and  $S_a$  for the ambient aerosol surface area density. For  $\text{NO}_2$  conversion on ground surface,  $\gamma_g$  is assumed to be  $1 \times 10^{-6}$  during nighttime and  $2 \times 10^{-5}$  during daytime and  $S/V$  is assumed to be  $0.1 \text{ m}^{-1}$  as in Vogel et al. (2003). Since no measurements of fog droplet surface areas were made in this experiment, we use a  $\gamma_a$  range of  $1 \times 10^{-4}$  to  $1 \times 10^{-3}$  as suggested by Li et al. (2018b) and a wide range of surface area densities to account for both aerosol and fog conditions. Additionally, for non-fog conditions, the ambient aerosol surface area density calculated using the simultaneously measured PNSD and aerosol hygroscopicity parameter derived from measurements of a humidified nephelometer system and  $\gamma_a = 1 \times 10^{-4}$  is applied to further calculate the variation of the HONO production on aerosol surface.

HONO loss through photolysis reactions were calculated as:

$$L_{pho} = J_{HONO}[\text{HONO}], \quad (\text{Eq.5})$$

where  $J_{HONO}$  was modelled using the TUV radiative transfer model (version 5.3, <http://www2.acom.ucar.edu/modeling/tuv>). The required single scattering albedo and aerosol angstrom exponent were estimated using simultaneously measured PNSD and BC measurements (Kuang et al., 2015), while the 550nm aerosol optical depth (AOD) was assumed to vary with RH (Table S1).

Loss through dry deposition was estimated using equation 6:

$$L_{dep} = \frac{v_{dep}}{H} [HONO], \quad (\text{Eq.6})$$

where the dry deposition rate  $v_{dep}$  was assumed to be  $0.3 \text{ cm s}^{-1}$  according to (Stutz et al., 2002) and the boundary layer height  $H$  was interpolated from ECWMF ERA-interim data (<http://apps.ecmwf.int/datasets/data/interim-full-daily/>).

The comparison between the calculated HONO net production rate and actually measured HONO variation rate ( $d[HONO]/dt$ ) is displayed in Fig. 5. The estimated upper limit for vehicle emissions displays little variability during the day, with slight decreasing trends during the four events, proving that the observed HONO production could not have been caused by direct vehicle emissions. The net gaseous phase production of HONO ( $P_{hom}^{net}$ ) contributed 0.15-0.18, 0.04-0.07, 0.27-1.04 and 0.25-1.53  $\text{ppb h}^{-1}$  during the 4 case events, displaying little influence during fog events and more during haze events. However, the estimated  $P_{hom}^{net}$  was far from sufficient to explain the observed  $d[HONO]/dt$ . Dry deposition was typically high during the night within the shallow nocturnal boundary layer and decreased during the day with the increase of the boundary layer height. The calculated  $L_{dep}$  contributed 0.5-0.9, 0.4-0.6, 2.7-4.3 and 0.05-0.3  $\text{ppb h}^{-1}$  to the loss of HONO. No significant decreases in  $L_{dep}$  were observed during the two fog events, while increases were detected during the cases on 11<sup>th</sup> and 14<sup>th</sup> Nov. Not only was the variation in  $L_{dep}$  unable to explain observed HONO productions, it further added to the discrepancy between observed and calculated  $d[HONO]/dt$ . During the four case events the  $J_{HONO}$  respectively increased from  $0.7 \times 10^{-4}$  to  $2.5 \times 10^{-4} \text{ s}^{-1}$ ,  $1.6 \times 10^{-4}$  to  $2.4 \times 10^{-4} \text{ s}^{-1}$ ,  $0.03 \times 10^{-4}$  to  $1.4 \times 10^{-4} \text{ s}^{-1}$  and  $1.6 \times 10^{-4}$  to  $4.4 \times 10^{-4} \text{ s}^{-1}$ , with  $L_{pho}$  contributing 0.9-8.9, 2.2-7.8, 0.03-5.5 and 0.8-26.4  $\text{ppb h}^{-1}$  to the loss of HONO.  $J_{HONO}$  increased significantly by the end of the HONO growth events to  $2.9 \times 10^{-4}$ ,  $4.3 \times 10^{-4}$ ,  $2.6 \times 10^{-4}$  and  $6.6 \times 10^{-4} \text{ s}^{-1}$ , respectively, suggesting that the rapid drop of HONO concentrations was high probably caused by the rapid photolysis. Overall,  $L_{pho}$  contributed most to the discrepancy between observed and calculated  $d[HONO]/dt$ .

Generally, the observed and calculated  $d[HONO]/dt$  agreed better with each other outside the HONO explosive growth periods, showing overestimations when aerosol liquid water contents were high, suggesting possible overestimation in the  $\text{NO}_2$  uptake coefficient in the parameterization of  $P_{het}$ . This further suggests that the observed discrepancies in HONO production have mainly been caused by uncertainties in the heterogeneous formation estimates. The fact that HONO drastically increased while  $\text{NO}_2$  varied little (9:30 to 11:30, 5<sup>th</sup> Nov. and 6:30

to 8:30, 11<sup>th</sup> Nov.) or hardly increased even under drastic increases of NO<sub>2</sub> (8:30 to 11:30, 14<sup>th</sup> Nov.), but displayed explosive growth with increasing NH<sub>3</sub>, could not be explained by current known HONO sources (direct emission or gas phase reactions). Additionally, these rapid increasing HONO phenomena were all observed under foggy or high RH conditions, which further affirms the suspicion that the HONO increase was caused by heterogeneous conversion of NO<sub>2</sub>.

#### 4.2 Heterogeneous HONO formation mechanism

As manifested in Sect. 4.1, the unknown HONO source and the overestimates in HONO production were both linked to our limited understanding on the heterogeneous HONO formation mechanism. In this section, we try to evaluate the relative contribution of the currently known heterogeneous HONO formation pathways (R1 and R2) and reveal the reason for their limitations in explaining the observed HONO growth.

To evaluate which process (R1 or R2) was dominating the heterogeneous production of HONO, we assume that HONO was produced in aerosol and fog water simultaneously via R1 and R2. Since measurements of fog liquid water content or fog droplet surface area density were not made, we cannot directly quantify the absolute HONO production in fog. However, we can make a few assumptions to compare the relatively HONO contribution via R1 and R2. First, it was assumed that the observed sulfate production ( $d[SVI]/dt$ ) was caused by the reaction of SO<sub>2</sub> with H<sub>2</sub>O<sub>2</sub>, O<sub>3</sub>, NO<sub>2</sub>, transition metal ions (TMI: Fe<sup>3+</sup> and Mn<sup>2+</sup>). Calculations were performed according to Cheng et al. (2016), using the same pH dependent TMI concentrations and the actually measured SO<sub>2</sub>, H<sub>2</sub>O<sub>2</sub>, O<sub>3</sub> and NO<sub>2</sub> concentrations (Table S2). For the two fog episodes on 4<sup>th</sup> and 5<sup>th</sup> Nov. 2016, the mean diameter of fog droplets was assumed to be 7.0  $\mu\text{m}$  and the liquid water content was assumed to be 0.3  $\text{g m}^{-3}$  according to Shen et al. (2018). For the haze episodes on the 11<sup>th</sup> and 14<sup>th</sup> Nov. 2016, the mean aerosol diameter under ambient conditions was estimated to be 0.65-1.22 and 0.9  $\mu\text{m}$ , while the liquid water content was calculated to decrease from  $3.4 \times 10^{-4}$  to  $7.8 \times 10^{-5} \text{ g m}^{-3}$  on the 11<sup>th</sup> Nov and assumed to be 0.01  $\text{g m}^{-3}$  on the 14<sup>th</sup> Nov. during the transition from fog to haze. The sulfate production rate and relative contribution of each oxidation pathway to the total sulfate production rate was obtained and depicted in Fig.6. For the two fog episodes, assuming pH=6, the estimated average sulfate production rates are 11.7 and 31.6  $\mu\text{g m}^{-3} \text{ h}^{-1}$  approximately 4 times of that observed within PM<sub>2.5</sub>, which might be an underestimation, considering the liquid water content of fog droplets are at least a magnitude higher than that of aerosols. For the two haze episodes, using the pH values estimated using ISORROPIA (forward

mode and metastable assumption (Song et al., 2018)), the estimated average sulfate production rates are 0.06 and 1.8  $\mu\text{g m}^{-3} \text{h}^{-1}$ , about 10% of that observed within  $\text{PM}_{2.5}$ . Following the calculations of Cheng et al. (2016), we have considered the influence of ionic strength on the reaction rates and set constraints on the maximum ionic strength ( $I_{\text{max}}$ ), which might have caused underestimations for all reaction routes, since the calculated ionic strength commonly exceeded  $I_{\text{max}}$ . Underestimated transition metal ion concentrations may also be partly responsible for the underpredicted sulfate production, since the TMI catalysis route has recently be pointed out to be the dominant  $\text{SO}_2$  heterogeneous oxidation pathway {Shao, 2019 #2155}. Additionally, there also might be other neglected  $\text{SO}_2$  oxidation pathways, which will lead to overestimates in the sulfate fraction produced by the  $\text{NO}_2$  oxidation pathway. Therefore, we can only yield an upper limit for the HONO production rate of R1:

$$\frac{d[\text{HONO}]}{dt}_{R1} = 2 \times \text{frac}_{\text{SO}_2+\text{NO}_2} \times \frac{d[\text{SVI}]}{dt}_{\text{obs}}, \quad (\text{Eq.7})$$

where  $\text{frac}_{\text{SO}_2+\text{NO}_2}$  is the contribution fraction of the  $\text{NO}_2$  oxidation pathway to the total sulfate production. Note that the calculated HONO production rate can only represent the production within  $\text{PM}_{2.5}$ .

By further assuming that all the observed nitrate production ( $d[\text{NO}_3^-]/dt$ ) was caused by reaction R2 and by the reaction of  $\text{NO}_2$  with OH radicals ( $k_{\text{NO}_2+\text{OH}}=3.2\times 10^{-12} \text{ cm}^3 \text{ s}^{-1}$ ), the HONO production rate of R2 would be:

$$\frac{d[\text{HONO}]}{dt}_{R2} = \frac{d[\text{NO}_3^-]}{dt}_{\text{obs}} - k_{\text{NO}_2+\text{OH}}[\text{NO}_2][\text{OH}]. \quad (\text{Eq.8})$$

The contribution fraction of the two reactions to the heterogeneous HONO production in aerosol and fog liquid water content can be calculated by:

$$f_{R1} = \frac{d[\text{HONO}]}{dt}_{R1} / \frac{d[\text{HONO}]}{dt}_{R1+R2} \quad \text{and} \quad (\text{Eq.9-1})$$

$$f_{R2} = \frac{d[\text{HONO}]}{dt}_{R2} / \frac{d[\text{HONO}]}{dt}_{R1+R2}. \quad (\text{Eq.9-2})$$

Assuming the pH of fog droplets falls within the range of 4 to 6,  $f_{R2}$  was estimated to range from range from 75.5 to 99.5% and from 81.2 to 99.5% during the 4<sup>th</sup> and 5<sup>th</sup> Nov. 2016,

respectively. For the two haze events on 11<sup>th</sup> and 14<sup>th</sup> Nov., the  $f_{R2}$  corresponding to the pH values modelled by ISORROPIA would be 98.2% and 97.3%.

These results suggest that, reaction R2 is the dominant contributor to the heterogeneous HONO production, while R1 is more important under high pH conditions. Under the assumed upper limit of pH, R1 can contribute up to 24.5%, 18.8% to the observed HONO growth during the fog events. This is in accordance with results from Wang et al. (2016) and Cheng et al. (2016), which suggested that R1 was more likely to happen during fog episodes or under NH<sub>3</sub> neutralized conditions (3,4). For the two haze events, R1 contributed very little (1.8% and 2.7%) to the observed HONO growth.

Since R2 seems to be the dominant contributor to the observed HONO production, it is important to evaluate whether the parameterizations in current literature can accurately describe the HONO production process of R2. The HONO production rate of R2 is typically parameterized as in Eq.4, where the NO<sub>2</sub> concentration and the surface area density of fog droplets/aerosol particles are the controlling factors of the NO<sub>2</sub> uptake, as opposed to the pH of the water droplets (Li et al., 2018b; Yabushita et al., 2009). Based on the reactive uptake coefficient of NO<sub>2</sub> ( $\gamma_{NO_2}$ ) in Yabushita et al. (2009) and Li et al. (2018b), we have calculated the HONO production rate of R2 under different conditions (Fig.S4). During foggy conditions, the HONO production rate should be higher than 1 ppb (ppb NO<sub>2</sub>·h)<sup>-1</sup>. The NO<sub>2</sub> concentration during the two fog episodes ranged between 40 to 50 ppb, therefore, the HONO production rate would have been higher than 40 ppb h<sup>-1</sup>. However, no rapid increase of HONO was observed unless NH<sub>3</sub> was simultaneously increasing. As already mentioned before, under hazy conditions,  $P_{het}$  significantly overestimated the HONO production when relative humidity was high and large ambient aerosol surface area densities were observed (Fig5), while it failed to reproduce the growth in HONO on the morning of the 11<sup>th</sup> Nov. 2016. These results indicate that R2 is missing the important impact of NH<sub>3</sub> in the heterogeneous HONO production and that the  $\gamma_{NO_2}$  range is at least overestimated when NH<sub>3</sub> is not abundant enough.

Recent theoretical simulation results ascertain that NH<sub>3</sub> can promote the hydrolysis of NO<sub>2</sub> and contribute to HONO formation via R2 (Li et al., 2018a). This conclusion is consistent with the observed phenomena that HONO only increased rapidly when NH<sub>3</sub> was simultaneously increasing. Considering the influence of NH<sub>3</sub> and sulfate on the aerosol pH, under our observed NH<sub>3</sub> concentration range, NH<sub>3</sub> has negligible impact on pH values (Guo et al., 2017), especially under

high RH conditions. This further proves that the  $\text{NH}_3$ -promoted hydrolysis of  $\text{NO}_2$  is independent of the pH value. Another phenomenon worth noting is that, in Case 3, HONO was increasing rapidly even under the drastic decrease in ambient RH, which demonstrates that the impact of  $\text{NH}_3$  on HONO formation should be even more important than that of aerosol liquid water content. However, the hydrolysis of  $\text{NO}_2$  needs water to be involved, thus, the importance of water content under different conditions remains to be elucidated.

To further investigate the acceleration effect of  $\text{NH}_3$  on the hydrolysis of  $\text{NO}_2$ , we have examined the correlations between the  $\text{NO}_2$ -to-HONO (HONO/ $\text{NO}_2$  ratio),  $\text{NO}_2$ -to- $\text{NO}_3^-$  ( $\text{NO}_3^-$ / $\text{NO}_2$  ratio) conversion efficiencies and the  $\text{NH}_3$  concentration during the entire field campaign (Fig.7). Note that only data points during nighttime (18 pm to 6 am) and with ambient RH higher than 80% are displayed in Fig.7. Daytime data were excluded, because HONO would quickly photolyze as soon as sunlight was available. Even if there was rapid HONO production, the corresponding increase of HONO might not be observable due to its quick photolysis. The reason for only including data with ambient RH higher than 80% is that the quick hydrolysis of  $\text{NO}_2$  requires water to be involved. However, the overall hygroscopicity of ambient aerosols during this field campaign was relatively low, with an average hygroscopicity parameter  $\kappa$  of 0.14, and the volume contribution of liquid water to the total volume concentrations of ambient aerosols was quite low when ambient RH is below 80% (Kuang et al., 2018). The correlation coefficient between HONO/ $\text{NO}_2$  ratio and the  $\text{NH}_3$  concentration reaches 0.68, while that between  $\text{NO}_3^-$ / $\text{NO}_2$  ratio and  $\text{NH}_3$  concentration only reaches 0.48, since the source of  $\text{NO}_3^-$  is much more complicated than that of HONO. These results have further verified that  $\text{NH}_3$  promotes the  $\text{NO}_2$  hydrolysis and HONO production. The correlation of HONO/ $\text{NO}_2$  to  $\text{NH}_3$  is highly nonlinear, HONO/ $\text{NO}_2$  increases rapidly with  $\text{NH}_3$  when  $\text{NH}_3$  reaches above 10 ppb.

#### **4.3 Feedback between HONO formation and inorganic secondary aerosol formation**

According to the discussions in Sect.4.2,  $\text{NH}_3$  promotes the hydrolysis of  $\text{NO}_2$ , producing nitrate and most of the observed HONO. However, the connection between the  $\text{NH}_3$  promoted hydrolysis and the simultaneous rapid sulfate production remains unexplained. As was already discussed in Sect.4.2, the sulfate production rate calculated based on currently known  $\text{SO}_2$  oxidation pathways largely underestimates the observed sulfate growth, indicating that there might be neglected oxidation pathways. Li et al. (2018b) pointed out that  $\text{NO}_2$  can oxidize S(IV)

indirectly via free radical mechanism (the involved reactions RS1 to RS5 proposed in Li et al. (2018b) listed in the supplement). The key step of the proposed S(IV) oxidation pathway is the photolysis of HONO to produce OH radicals (RS1). OH can oxidize S(IV) to form bisulfate or sulfate through reaction RS2 and produce HO<sub>2</sub>. HO<sub>2</sub> can react with NO to produce NO<sub>2</sub>, or react with itself to produce H<sub>2</sub>O<sub>2</sub>. As was depicted in Fig.5, the radiation during the fog/haze events was already strong enough to photolyze the produced HONO and release OH radicals at the same rates as  $L_{pho}$  in Sect. 4.1, indicating there was strong OH production, especially near the end of the events. For the two fog events, no AOD measurements were available. Assuming AOD=2.5 for foggy conditions, the lifetime of HONO (only considering the photolysis process) were estimated to decrease from 4.2 to 1.1 h, 1.7 to 1.1 h during the growth of HONO and to drop to 1.0 and 0.7 h by the time of the drastic decreases in HONO. In the haze event on the 11<sup>th</sup> Nov., AOD measurements were also not available due to cloud coverage, however, sensitivity study shows that the calculated HONO lifetime are much more sensitive to the AOD as opposed to the COD values (increasing 3.1 and 0.4 h per 0.1 increase in AOD and COD, Fig.S5). The HONO lifetime dropped from 2.0 h (by the time of the HONO peak) to 1.1 h (by time of the HONO decrease). During the case on the 14<sup>th</sup> Nov. 2016, the relative humidity decreased from 100% (10:00-11:00) to 86% (11:30), suggesting that this was a fog dissipation process. The HONO lifetime was estimated to be 1.7 h between 10:00 to 11:00, proving that the photolysis process was relatively weaker during the rapid increase of HONO. The estimated HONO lifetime rapidly decreased to 0.6 h by 12:00, resulting in accelerated HONO dissociation and OH production. The increase in H<sub>2</sub>O<sub>2</sub> observed during and after the increase of HONO, might be an indirect evidence of the HO<sub>2</sub> production and occurrence of RS2. The observed H<sub>2</sub>O<sub>2</sub> concentrations were much higher than the assumptions of 0.01 ppb made in Cheng et al. (2016), which was also pointed out by Ye et al. (2018). Under the assumed pH range for fog and the calculated pH range for aerosol, the estimated sulfate production was dominated by the SO<sub>2</sub> oxidation via H<sub>2</sub>O<sub>2</sub> (Fig.6). This indicates that both the calculated and the yet unexplained sulfate production were linked to the photolysis of HONO.

NH<sub>3</sub> promoted the hydrolysis of NO<sub>2</sub>, producing HONO and nitrate. HONO easily photolyzes releasing OH radicals, which further converted to HO<sub>2</sub> and H<sub>2</sub>O<sub>2</sub>. The highly oxidative free radicals and H<sub>2</sub>O<sub>2</sub> collaboratively boosted the formation of sulfate. Hence, diurnal variations of NH<sub>3</sub> should have exerted significant influences on the diurnal variations of HONO and inorganic aerosol chemical components (sulfate, nitrate and ammonium, SNA). The average diurnal variations of



NO<sub>2</sub>, NH<sub>3</sub>, HONO as well as SO<sub>2</sub> concentrations during this field campaign are shown in Fig.8a. The average HONO concentration during nighttime is higher than that during daytime due to the quick photolysis of HONO upon solar irradiation. The NH<sub>3</sub> concentration begins to increase in the morning (near 8:00 LT) and reaches a plateau in the afternoon (8.5 to 15.5 ppb in average), and the SO<sub>2</sub> concentrations show a similar diurnal variation to that of NH<sub>3</sub>. This type of diurnal variation of SO<sub>2</sub> was also found by Xu et al. (2014), however, the cause of the common diurnal pattern between NH<sub>3</sub> and SO<sub>2</sub> during this field campaign requires further investigation. The NO<sub>2</sub> concentration increases quickly in the afternoon and decreases in the evening.

As shown in Fig.8b, the increase of NH<sub>3</sub> from morning to the afternoon was accompanied with the increase of mass fractions of nitrate and sulfate in PM<sub>2.5</sub> (The mass fractions of different aerosol chemical compositions were obtained by using the measured dry state PNSD to calculate volume concentration of PM<sub>2.5</sub>, assuming that the density of aerosols in dry state is 1.5 g cm<sup>-3</sup> (Yin et al., 2015)). The results shown in Fig.8b indicate that the molecular concentration increase in nitrate from the morning to the afternoon is much faster than that of sulfate, again supporting the fact that the NH<sub>3</sub>-promoted NO<sub>2</sub> hydrolysis, which only produces HONO and nitrate directly, was the main contributor to the observed explosive HONO formation. The evident morning increase of inorganic aerosol component fractions resulted in prominent increases of aerosol hygroscopicity, displaying an average  $\kappa$  anomaly of +0.04 during noontime (Fig.8c). From the morning to the afternoon, the ambient RH decreases quickly, however, the increase of aerosol hygroscopicity can retard the decrease of aerosol liquid water content and surface area density of ambient aerosols. This might act as a positive feedback, further enhancing the hydrolysis of NO<sub>2</sub> as well as the nitrate and sulfate formation.

## 5. Summary and atmospheric implications

Explosive HONO growth (observed maximum  $d[\text{HONO}]/dt=16.1 \text{ ppb h}^{-1}$ ) was observed for the first time on the NCP during fog and haze episodes with high RH conditions, only occurring with evident increases in NH<sub>3</sub>, indicating that NH<sub>3</sub> is the key factor promoting the hydrolysis of NO<sub>2</sub>, resulting in rapid HONO and nitrate formation. NH<sub>3</sub> concentrations during the observation period exhibit a distinct diurnal variation with an increase in the morning and a peak in the afternoon (8.5 to 15.5 ppb in average). The increase of NH<sub>3</sub> promotes the hydrolysis of NO<sub>2</sub>, giving significant rise to HONO and nitrate concentrations. Produced HONO releases OH radicals upon photolysis, which further oxidizes SO<sub>2</sub> to sulfate through gas phase and heterogeneous reactions.

Therefore, the significant growth of  $\text{NH}_3$  in the morning determined the increase in nitrate, sulfate and ammonium as well as that of aerosol hygroscopicity, which as a positive feedback retards the decrease in atmospheric liquid water content and further enhances the hydrolysis of  $\text{NO}_2$  as well as the nitrate and sulfate formation.

Results in this paper reveals that the  $\text{NH}_3$ -promoted  $\text{NO}_2$  hydrolysis is a significant source of HONO, which provides direct insight into the missing daytime source of HONO on the NCP. Results in this paper also shed light on the recent controversy of how  $\text{SO}_2$ , pH and  $\text{NH}_3$  are involved in heterogeneous HONO production. It was clarified that in the HONO production,  $\text{SO}_2$  took a minor part during fog events and an insignificant part during haze events, the observed growth in sulfate was dominantly the byproduct of the HONO photolysis, confirming again the importance HONO as an OH source and its crucial role in atmospheric chemistry.

These results have demonstrated the critical role and contribution of  $\text{NH}_3$  in the formation of photochemical and aerosol pollution on the North China Plain. Effective control measures are urgently called for to reduce  $\text{NH}_3$  emissions, which would simultaneously benefit the photochemical and aerosol pollution abatement through the reduction of HONO production.

## Acknowledgments, Samples, and Data

This work is supported by the National Key R&D Program of China (2016YFC0202300), the National research program for key issues in air pollution control (DQGG0103) and the National Natural Science Foundation of China (41505107 and 41590872). We thank Wei Peng from Beijing Met High-Tech Co., Ltd. for his help with the maintenance of the IGAC instrument.

**Data availability.** The data used in this study are available from the corresponding author upon request (kuangye@jnu.edu.cn)

## References

- Cheng, Y., Zheng, G., Wei, C., Mu, Q., Zheng, B., Wang, Z., Gao, M., Zhang, Q., He, K., Carmichael, G., Pöschl, U., and Su, H.: Reactive nitrogen chemistry in aerosol water as a source of sulfate during haze events in China, *Science Advances*, 2, e1601530, 10.1126/sciadv.1601530, 2016.
- Cui, L., Li, R., Zhang, Y., Meng, Y., Fu, H., and Chen, J.: An observational study of nitrous acid (HONO) in Shanghai, China: The aerosol impact on HONO formation during the haze episodes, *The Science of the total environment*, 630, 1057-1070, 10.1016/j.scitotenv.2018.02.063, 2018.
- Ding, J., Zhao, P., Su, J., Dong, Q., and Du, X.: Aerosol pH and its influencing factors in Beijing, *Atmos. Chem. Phys. Discuss.*, 2018, 1-34, 10.5194/acp-2018-270, 2018.

Guo, H., Weber, R. J., and Nenes, A.: High levels of ammonia do not raise fine particle pH sufficiently to yield nitrogen oxide-dominated sulfate production, *Scientific reports*, 7, 12109, 10.1038/s41598-017-11704-0, 2017.

Huang, R.-J., Yang, L., Cao, J., Wang, Q., Tie, X., Ho, K.-F., Shen, Z., Zhang, R., Li, G., Zhu, C., Zhang, N., Dai, W., Zhou, J., Liu, S., Chen, Y., Chen, J., and O'Dowd, C. D.: Concentration and sources of atmospheric nitrous acid (HONO) at an urban site in Western China, *Science of The Total Environment*, 593-594, 165-172, <https://doi.org/10.1016/j.scitotenv.2017.02.166>, 2017.

Kleffmann, J., Gavriloaiei, T., Hofzumahaus, A., Holland, F., Koppmann, R., Rupp, L., Schlosser, E., Siese, M., and Wahner, A.: Daytime formation of nitrous acid: A major source of OH radicals in a forest, *Geophysical Research Letters*, 32, doi:10.1029/2005GL022524, 2005.

Kuang, Y., Zhao, C. S., Tao, J. C., and Ma, N.: Diurnal variations of aerosol optical properties in the North China Plain and their influences on the estimates of direct aerosol radiative forcing, *Atmos. Chem. Phys. Discuss.*, 15, 339-369, 10.5194/acpd-15-339-2015, 2015.

Kuang, Y., Zhao, C., Tao, J., Bian, Y., Ma, N., and Zhao, G.: A novel method for deriving the aerosol hygroscopicity parameter based only on measurements from a humidified nephelometer system, *Atmos. Chem. Phys.*, 17, 6651-6662, 10.5194/acp-17-6651-2017, 2017.

Kuang, Y., Zhao, C. S., Zhao, G., Tao, J. C., Xu, W., Ma, N., and Bian, Y. X.: A novel method for calculating ambient aerosol liquid water content based on measurements of a humidified nephelometer system, *Atmospheric Measurement Techniques*, 11, 2967-2982, 10.5194/amt-11-2967-2018, 2018.

Li, L., Duan, Z., Li, H., Zhu, C., Henkelman, G., Francisco, J. S., and Zeng, X. C.: Formation of HONO from the NH<sub>3</sub>-promoted hydrolysis of NO<sub>2</sub>-dimers in the atmosphere, *Proceedings of the National Academy of Sciences*, 10.1073/pnas.1807719115, 2018a.

Li, L., Hoffmann, M. R., and Colussi, A. J.: Role of Nitrogen Dioxide in the Production of Sulfate during Chinese Haze-Aerosol Episodes, *Environmental Science & Technology*, 52, 2686-2693, 10.1021/acs.est.7b05222, 2018b.

Li, X., Brauers, T., Häseler, R., Bohn, B., Fuchs, H., Hofzumahaus, A., Holland, F., Lou, S., Lu, K. D., Rohrer, F., Hu, M., Zeng, L. M., Zhang, Y. H., Garland, R. M., Su, H., Nowak, A., Wiedensohler, A., Takegawa, N., Shao, M., and Wahner, A.: Exploring the atmospheric chemistry of nitrous acid (HONO) at a rural site in Southern China, *Atmospheric Chemistry and Physics*, 12, 1497-1513, 10.5194/acp-12-1497-2012, 2012.

Liu, M., Song, Y., Zhou, T., Xu, Z., Yan, C., Zheng, M., Wu, Z., Hu, M., Wu, Y., and Zhu, T.: Fine particle pH during severe haze episodes in northern China, *Geophysical Research Letters*, 44, 5213-5221, doi:10.1002/2017GL073210, 2017a.

Liu, Y., Wu, Z., Wang, Y., Xiao, Y., Gu, F., Zheng, J., Tan, T., Shang, D., Wu, Y., Zeng, L., Hu, M., Bateman, A. P., and Martin, S. T.: Submicrometer Particles Are in the Liquid State during Heavy Haze Episodes in the Urban Atmosphere of Beijing, China, *Environmental Science & Technology Letters*, 4, 427-432, 10.1021/acs.estlett.7b00352, 2017b.

Liu, Z., Wang, Y., Costabile, F., Amoroso, A., Zhao, C., Huey, L. G., Stickel, R., Liao, J., and Zhu, T.: Evidence of Aerosols as a Media for Rapid Daytime HONO Production over China, *Environmental Science & Technology*, 48, 14386-14391, 10.1021/es504163z, 2014.

Lu, C., Niu, S., Tang, L., Lv, J., Zhao, L., and Zhu, B.: Chemical composition of fog water in Nanjing area of China and its related fog microphysics, *Atmospheric Research*, 97, 47-69, <http://dx.doi.org/10.1016/j.atmosres.2010.03.007>, 2010.

Lu, K., Guo, S., Tan, Z., Wang, H., Shang, D., Liu, Y., Li, X., Wu, Z., Hu, M., and Zhang, Y.: Exploring atmospheric free-radical chemistry in China: the self-cleansing capacity and the

formation of secondary air pollution, *National Science Review*, nwy073-nwy073, 10.1093/nsr/nwy073, 2018.

Meng, Z., Xu, X., Lin, W., Ge, B., Xie, Y., Song, B., Jia, S., Zhang, R., Peng, W., Wang, Y., Cheng, H., Yang, W., and Zhao, H.: Role of ambient ammonia in particulate ammonium formation at a rural site in the North China Plain, *Atmos. Chem. Phys.*, 18, 167-184, 10.5194/acp-18-167-2018, 2018.

Michoud, V., Colomb, A., Borbon, A., Miet, K., Beekmann, M., Camredon, M., Aumont, B., Perrier, S., Zapf, P., Siour, G., Ait-Helal, W., Afif, C., Kukui, A., Furger, M., Dupont, J. C., Haefelin, M., and Doussin, J. F.: Study of the unknown HONO daytime source at a European suburban site during the MEGAPOLI summer and winter field campaigns, *Atmos. Chem. Phys.*, 14, 2805-2822, 10.5194/acp-14-2805-2014, 2014.

Nie, W., Ding, A. J., Xie, Y. N., Xu, Z., Mao, H., Kerminen, V. M., Zheng, L. F., Qi, X. M., Huang, X., Yang, X. Q., Sun, J. N., Herrmann, E., Petäjä, T., Kulmala, M., and Fu, C. B.: Influence of biomass burning plumes on HONO chemistry in eastern China, *Atmos. Chem. Phys.*, 15, 1147-1159, 10.5194/acp-15-1147-2015, 2015.

Petters, M. D., and Kreidenweis, S. M.: A single parameter representation of hygroscopic growth and cloud condensation nucleus activity, *Atmospheric Chemistry and Physics*, 7, 1961-1971, 2007.

Ran, L., Zhao, C. S., Xu, W. Y., Lu, X. Q., Han, M., Lin, W. L., Yan, P., Xu, X. B., Deng, Z. Z., Ma, N., Liu, P. F., Yu, J., Liang, W. D., and Chen, L. L.: VOC reactivity and its effect on ozone production during the HaChi summer campaign, *Atmos. Chem. Phys.*, 11, 4657-4667, 10.5194/acp-11-4657-2011, 2011.

Safai, P. D., Kewat, S., Pandithurai, G., Praveen, P. S., Ali, K., Tiwari, S., Rao, P. S. P., Budhawant, K. B., Saha, S. K., and Devara, P. C. S.: Aerosol characteristics during winter fog at Agra, North India, *J. Atmos. Chem.*, 61, 101-118, 10.1007/s10874-009-9127-4, 2008.

Shen, C., Zhao, C., Ma, N., Tao, J., Zhao, G., Yu, Y., and Kuang, Y.: Method to Estimate Water Vapor Supersaturation in the Ambient Activation Process Using Aerosol and Droplet Measurement Data, *Journal of Geophysical Research: Atmospheres*, 123, 10606-10619, doi:10.1029/2018JD028315, 2018.

Song, S., Gao, M., Xu, W., Shao, J., Shi, G., Wang, S., Wang, Y., Sun, Y., and McElroy, M. B.: Fine-particle pH for Beijing winter haze as inferred from different thermodynamic equilibrium models, *Atmos. Chem. Phys.*, 18, 7423-7438, 10.5194/acp-18-7423-2018, 2018.

Stutz, J., Alicke, B., and Neftel, A.: Nitrous acid formation in the urban atmosphere: Gradient measurements of NO<sub>2</sub> and HONO over grass in Milan, Italy, *Journal of Geophysical Research: Atmospheres*, 107, LOP 5-1-LOP 5-15, doi:10.1029/2001JD000390, 2002.

Su, H., Cheng, Y., Oswald, R., Behrendt, T., Trebs, I., Meixner, F. X., Andreae, M. O., Cheng, P., Zhang, Y., and Pöschl, U.: Soil Nitrite as a Source of Atmospheric HONO and OH Radicals, *Science*, 333, 1616-1618, 10.1126/science.1207687, 2011.

Teng, X., Hu, Q., Zhang, L., Qi, J., Shi, J., Xie, H., Gao, H., and Yao, X.: Identification of Major Sources of Atmospheric NH<sub>3</sub> in an Urban Environment in Northern China During Wintertime, *Environmental Science & Technology*, 51, 6839-6848, 10.1021/acs.est.7b00328, 2017.

Vogel, B., Vogel, H., Kleffmann, J., and Kurtenbach, R.: Measured and simulated vertical profiles of nitrous acid—Part II. Model simulations and indications for a photolytic source, *Atmospheric Environment*, 37, 2957-2966, [https://doi.org/10.1016/S1352-2310\(03\)00243-7](https://doi.org/10.1016/S1352-2310(03)00243-7), 2003.

Wang, G., Zhang, R., Gomez, M. E., Yang, L., Levy Zamora, M., Hu, M., Lin, Y., Peng, J., Guo, S., Meng, J., Li, J., Cheng, C., Hu, T., Ren, Y., Wang, Y., Gao, J., Cao, J., An, Z., Zhou, W., Li, G., Wang, J., Tian, P., Marrero-Ortiz, W., Secrest, J., Du, Z., Zheng, J., Shang, D., Zeng, L., Shao,

M., Wang, W., Huang, Y., Wang, Y., Zhu, Y., Li, Y., Hu, J., Pan, B., Cai, L., Cheng, Y., Ji, Y., Zhang, F., Rosenfeld, D., Liss, P. S., Duce, R. A., Kolb, C. E., and Molina, M. J.: Persistent sulfate formation from London Fog to Chinese haze, *Proceedings of the National Academy of Sciences*, 10.1073/pnas.1616540113, 2016.

Whalley, L. K., Stone, D., George, I. J., Mertes, S., van Pinxteren, D., Tilgner, A., Herrmann, H., Evans, M. J., and Heard, D. E.: The influence of clouds on radical concentrations: observations and modelling studies of HO<sub>x</sub> during the Hill Cap Cloud Thuringia (HCCT) campaign in 2010, *Atmos. Chem. Phys.*, 15, 3289-3301, 10.5194/acp-15-3289-2015, 2015.

Wu, Z., Wang, Y., Tan, T., Zhu, Y., Li, M., Shang, D., Wang, H., Lu, K., Guo, S., Zeng, L., and Zhang, Y.: Aerosol Liquid Water Driven by Anthropogenic Inorganic Salts: Implying Its Key Role in Haze Formation over the North China Plain, *Environmental Science & Technology Letters*, 10.1021/acs.estlett.8b00021, 2018.

Xing, J., Ding, D., Wang, S., Zhao, B., Jang, C., Wu, W., Zhang, F., Zhu, Y., and Hao, J.: Quantification of the enhanced effectiveness of NO<sub>x</sub> control from simultaneous reductions of VOC and NH<sub>3</sub> for reducing air pollution in the Beijing–Tianjin–Hebei region, China, *Atmos. Chem. Phys.*, 18, 7799-7814, 10.5194/acp-18-7799-2018, 2018.

Xu, W. Y., Zhao, C. S., Ran, L., Lin, W. L., Yan, P., and Xu, X. B.: SO<sub>2</sub> noontime-peak phenomenon in the North China Plain, *Atmospheric Chemistry and Physics*, 14, 7757-7768, 10.5194/acp-14-7757-2014, 2014.

Xue, L. K., Wang, T., Gao, J., Ding, A. J., Zhou, X. H., Blake, D. R., Wang, X. F., Saunders, S. M., Fan, S. J., Zuo, H. C., Zhang, Q. Z., and Wang, W. X.: Ground-level ozone in four Chinese cities: precursors, regional transport and heterogeneous processes, *Atmos. Chem. Phys.*, 14, 13175-13188, 10.5194/acp-14-13175-2014, 2014.

Yabushita, A., Enami, S., Sakamoto, Y., Kawasaki, M., Hoffmann, M. R., and Colussi, A. J.: Anion-Catalyzed Dissolution of NO<sub>2</sub> on Aqueous Microdroplets, *The Journal of Physical Chemistry A*, 113, 4844-4848, 10.1021/jp900685f, 2009.

Ye, C., Liu, P., Ma, Z., Xue, C., Zhang, C., Zhang, Y., Liu, J., Liu, C., Sun, X., and Mu, Y.: High H<sub>2</sub>O<sub>2</sub> Concentrations Observed during Haze Periods during the Winter in Beijing: Importance of H<sub>2</sub>O<sub>2</sub> Oxidation in Sulfate Formation, *Environmental Science & Technology Letters*, 10.1021/acs.estlett.8b00579, 2018.

Yin, Z., Ye, X., Jiang, S., Tao, Y., Shi, Y., Yang, X., and Chen, J.: Size-resolved effective density of urban aerosols in Shanghai, *Atmospheric Environment*, 100, 133-140, <http://dx.doi.org/10.1016/j.atmosenv.2014.10.055>, 2015.

Young, L.-H., Li, C.-H., Lin, M.-Y., Hwang, B.-F., Hsu, H.-T., Chen, Y.-C., Jung, C.-R., Chen, K.-C., Cheng, D.-H., Wang, V.-S., Chiang, H.-C., and Tsai, P.-J.: Field performance of a semi-continuous monitor for ambient PM<sub>2.5</sub> water-soluble inorganic ions and gases at a suburban site, *Atmospheric Environment*, 144, 376-388, <https://doi.org/10.1016/j.atmosenv.2016.08.062>, 2016.

Zheng, G. J., Duan, F. K., Su, H., Ma, Y. L., Cheng, Y., Zheng, B., Zhang, Q., Huang, T., Kimoto, T., Chang, D., Pöschl, U., Cheng, Y. F., and He, K. B.: Exploring the severe winter haze in Beijing: the impact of synoptic weather, regional transport and heterogeneous reactions, *Atmos. Chem. Phys.*, 15, 2969-2983, 10.5194/acp-15-2969-2015, 2015.



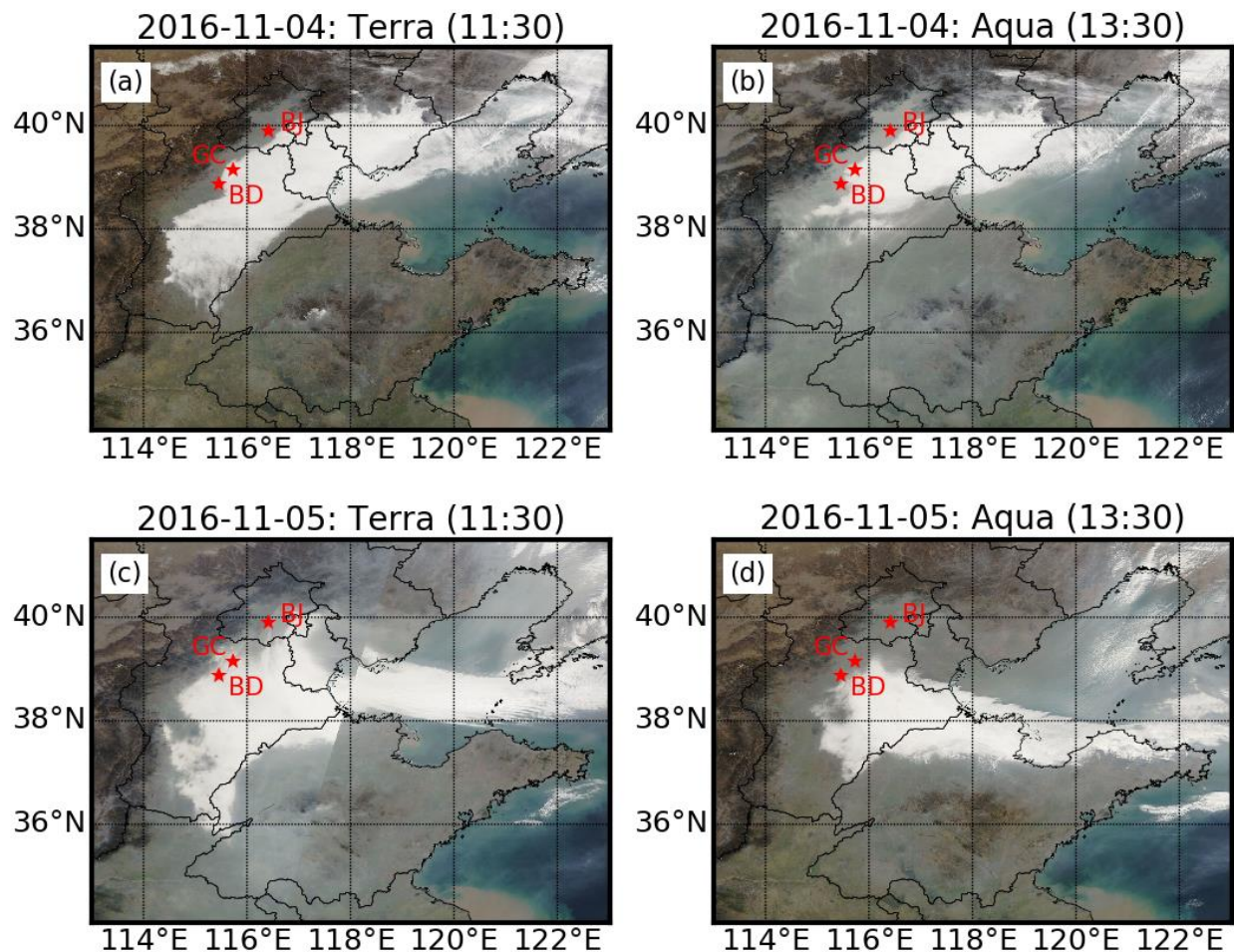


**Figure 1.** MODIS Terra (a,c) and Aqua (b,d) satellite images in 04<sup>th</sup> Nov. (a,b) and 5<sup>th</sup> Nov. 2016 (c,d), star markers are locations of Gucheng (GC: the observation site), Baoding (BD) and Beijing (BJ).

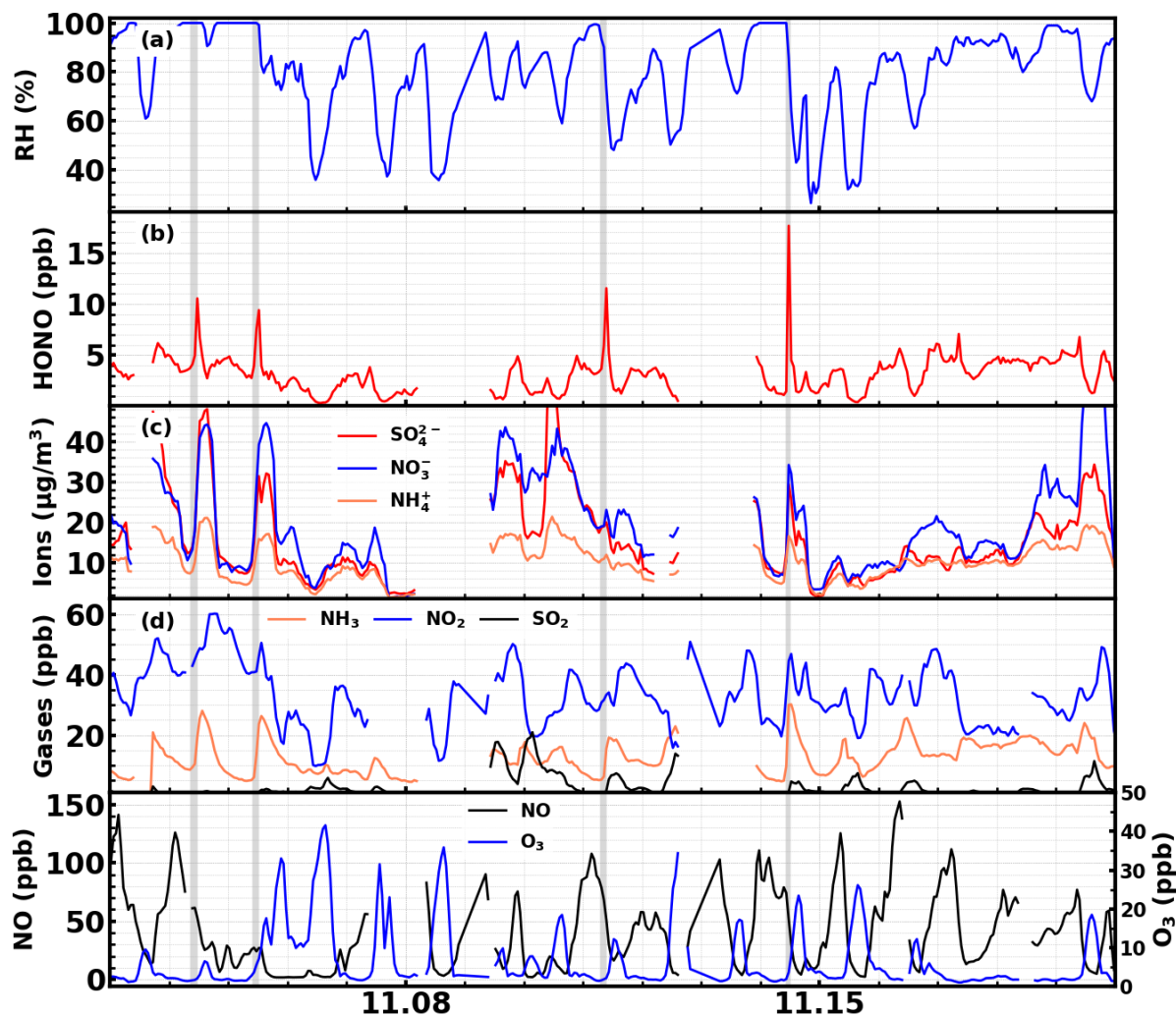


**Figure 2.** Time series of ambient **a)** RH; **b)** HONO; **c)** sulfate, nitrate, ammonium; **d)** NH<sub>3</sub>, NO<sub>3</sub> and SO<sub>2</sub> during the observation period.

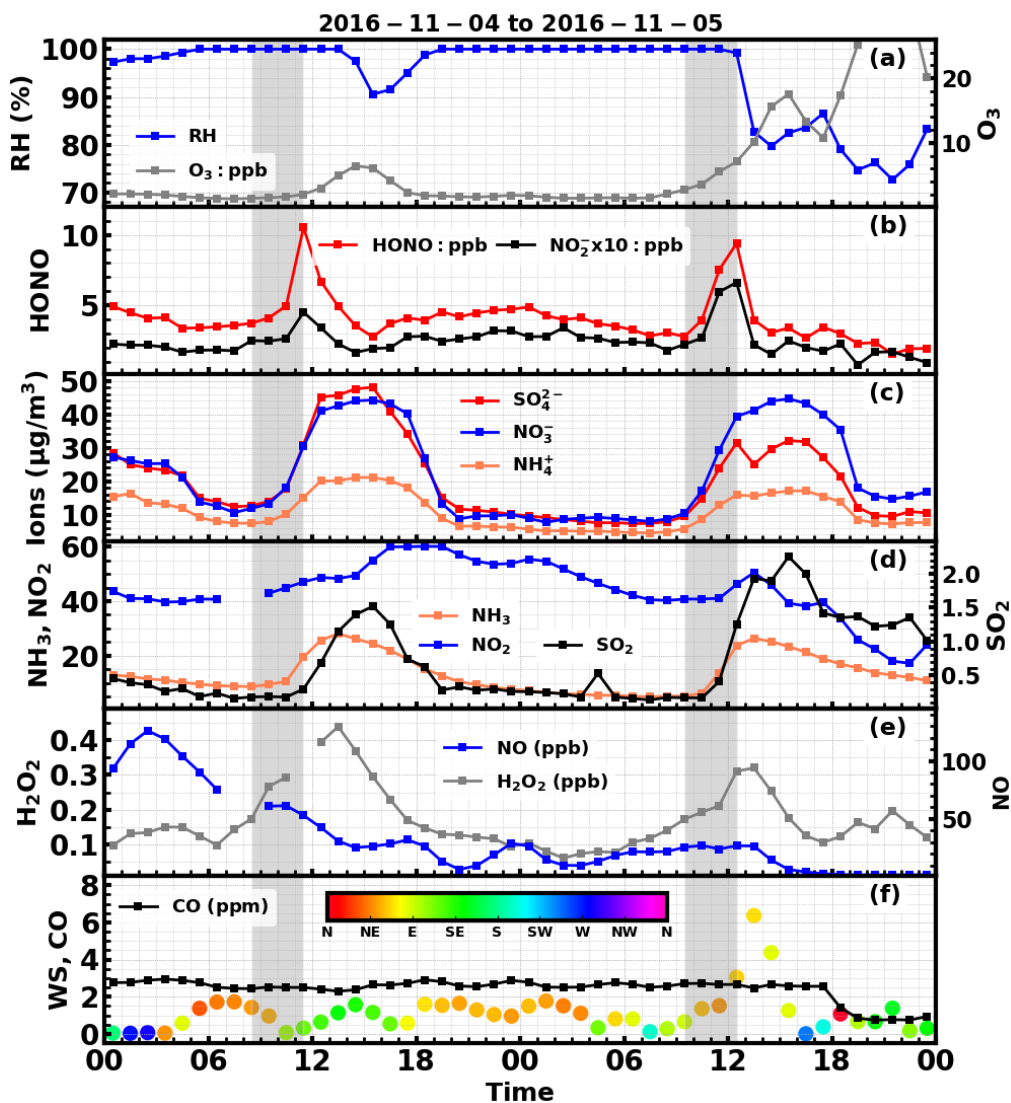


**Figure 3.** Time series of ambient a) RH, O<sub>3</sub>, b) HONO, NO<sub>2</sub>, c) SO<sub>4</sub><sup>2-</sup>, NO<sub>3</sub><sup>-</sup>, NH<sub>4</sub><sup>+</sup>, d) NH<sub>3</sub>, NO<sub>2</sub>, SO<sub>2</sub>, e) NO, H<sub>2</sub>O<sub>2</sub>, f) CO, wind speed and wind direction (colors of scatter points) from 4<sup>th</sup> to 5<sup>th</sup> Nov. 2016. Gray shaded areas represent periods of rapid increase of HONO.



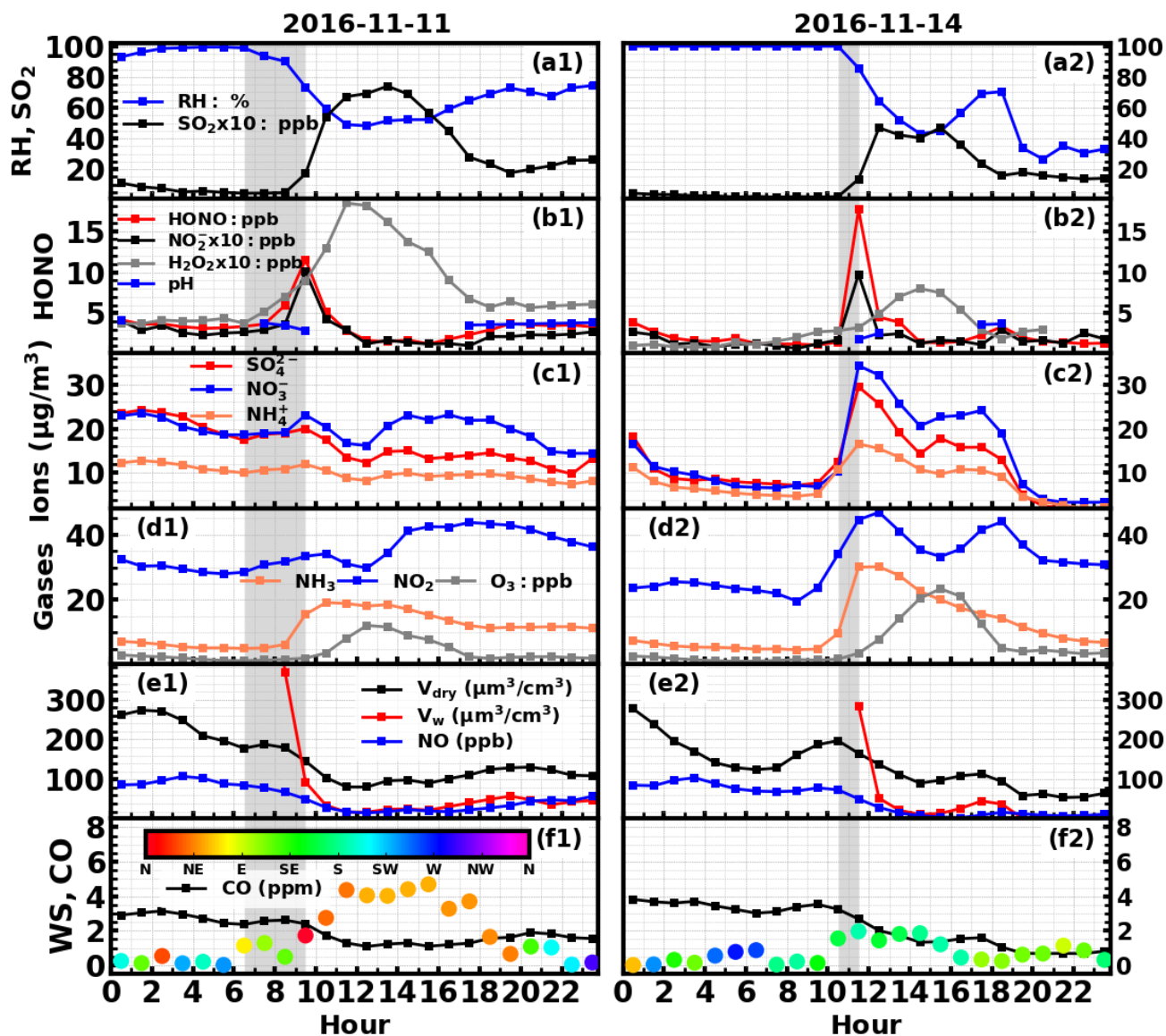


**Figure 4.** Time series of ambient **a)** RH, SO<sub>2</sub>, **b)** HONO, NO<sub>2</sub><sup>-</sup>, H<sub>2</sub>O<sub>2</sub>, aerosol pH, **c)** SO<sub>4</sub><sup>2-</sup>, NO<sub>3</sub><sup>-</sup>, NH<sub>4</sub><sup>+</sup>, **d)** NH<sub>3</sub>, NO<sub>2</sub>, O<sub>3</sub>, **e)** NO, volume concentrations of PM<sub>2.5</sub> in dry state (V<sub>dry</sub>), volume concentrations of liquid water (V<sub>w</sub>), **f)** CO, wind speed and wind direction during **1)** 11<sup>th</sup> Nov. 2016 and **2)** 14<sup>th</sup> Nov. 2016. Gray shaded areas represents periods of rapid increase of HONO.

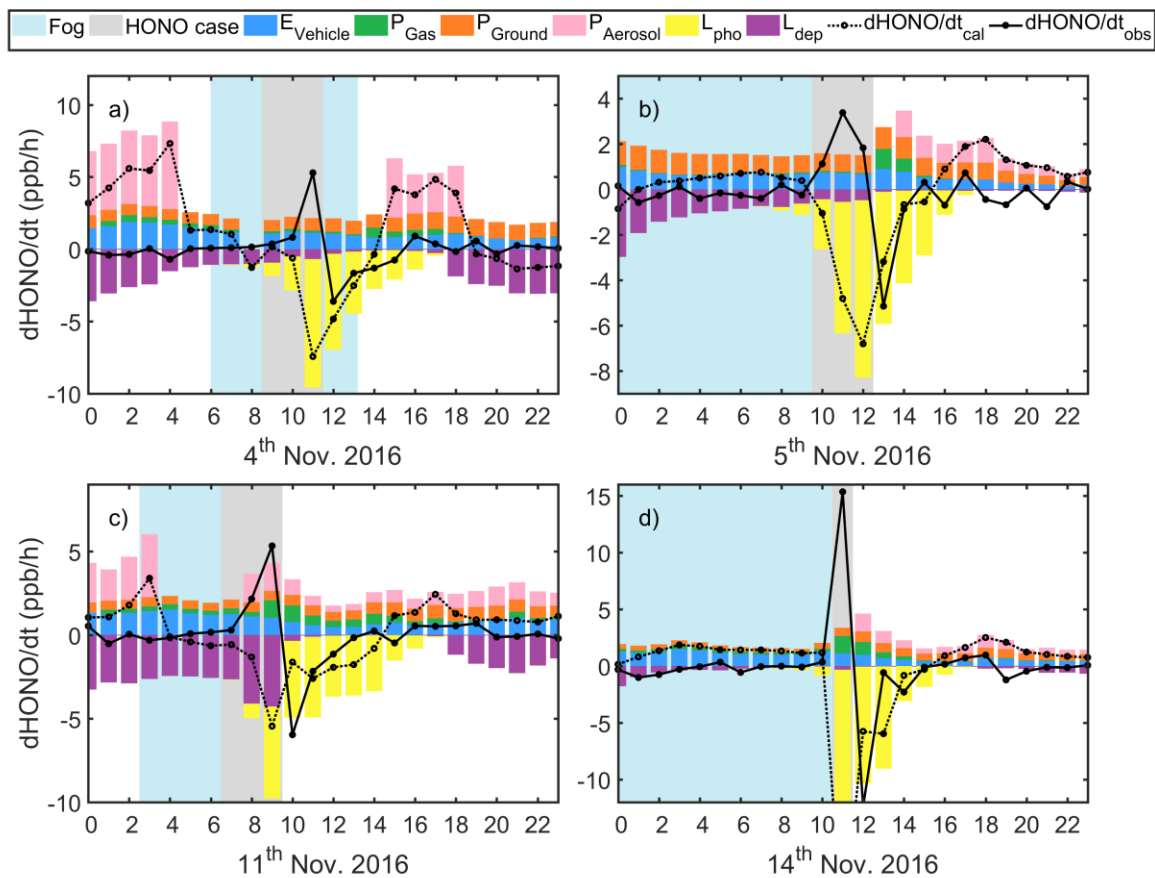


**Figure 5.** Estimated HONO emission from vehicles (blue), gas phase production (green), production on ground (orange) and aerosol surface (pink), loss through photolysis (yellow) and dry deposition (purple), as well as the calculated (dotted black) and actually observed (solid black)  $d[\text{HONO}]/dt$  on a) 4<sup>th</sup>, b) 5<sup>th</sup>, c) 11<sup>th</sup> and d) 14<sup>th</sup> Nov. 2016

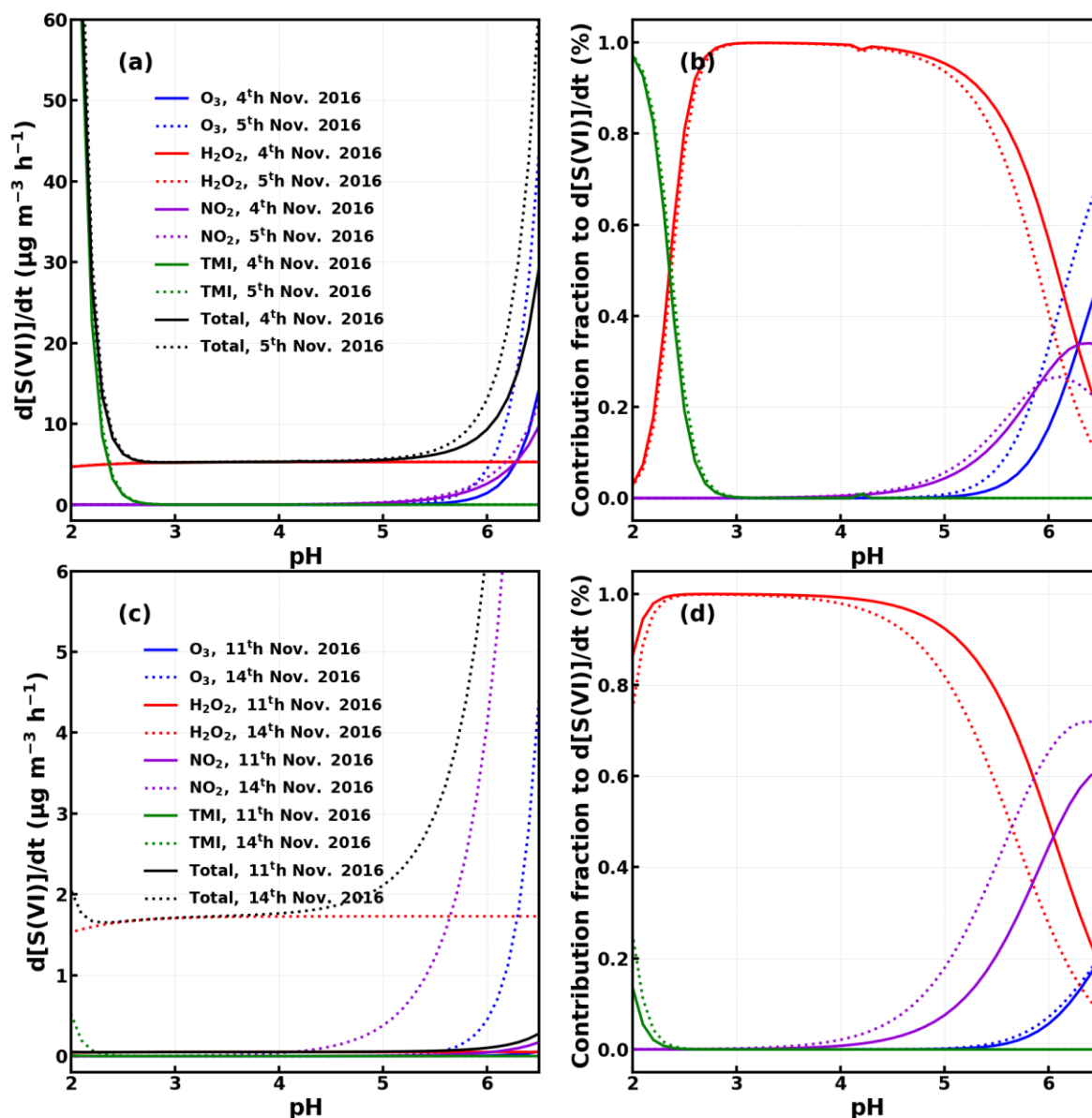


**Figure 6.** Calculated average sulfate production (a,c) and contribution fraction b,d) from SO<sub>2</sub> oxidation by H<sub>2</sub>O<sub>2</sub>, NO<sub>2</sub>, O<sub>3</sub>, TMI under different pH values using methods described in (Cheng et al., 2016) for the case episodes on 4<sup>th</sup>, 5<sup>th</sup>, 11<sup>th</sup> and 14<sup>th</sup> Nov. 2016.

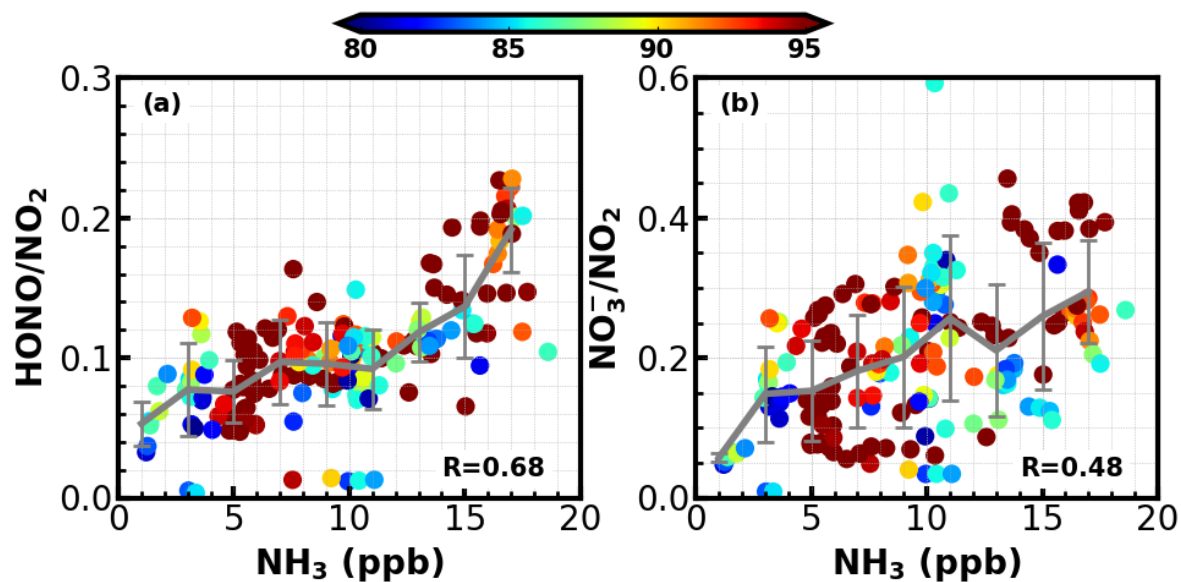


**Figure 7.** The relationship between  $\text{NH}_3$  concentration and **a)**  $\text{HONO}/\text{NO}_2$  ratio; **b)** nitrate/nitrogen dioxide ratio ( $\text{NO}_3^-/\text{NO}_2$ ); Colors of scatter points represent ambient RHs and the color bar is shown on the top.

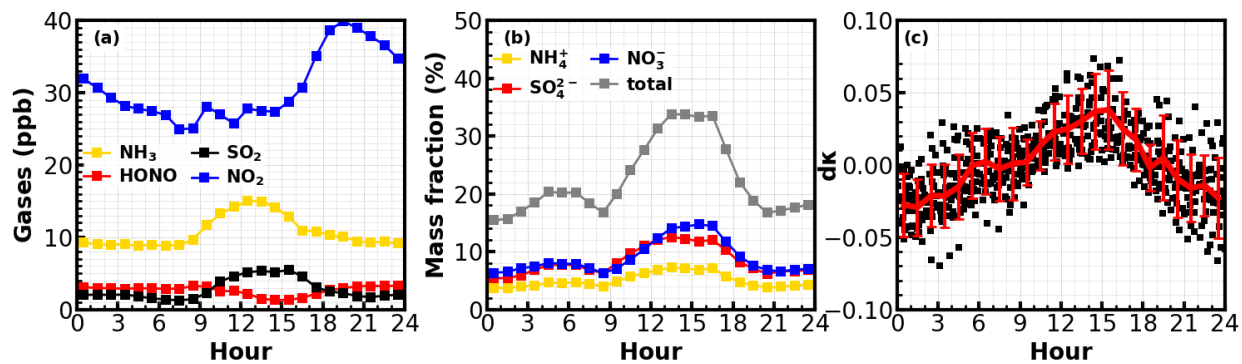


**Figure 8.** (a) Average diurnal variations of Gases; (b) Average diurnal variations mass fractions of nitrate, sulfate and ammonium; (c) Diurnal variations of aerosol hygroscopicity,  $\text{d}\kappa$  is the anomaly to the daily mean  $\kappa$ .